

Aerodynamic Noise Simulation of a Car Side Mirror at High Speed

Cong-Truong DINH*, The-Mich NGUYEN

School of Mechanical Engineering, Hanoi University of Science and Technology, Hanoi, Vietnam

*Corresponding author email: truong.dinhcong@hust.edu.vn

Abstract

Airflow around the car side mirrors is one of the sensitivity zones in which the airflow is separated and detached from the mirror flat side. The turbulence created by this flow detachment can affect the airflow to the main body of the car which lies behind the mirror. The turbulent structures of airflow exert directly on the lateral panels that causes the reduction of the car performance due to the increased drag, the source of noise and vibration, and so on. Consequently, the analysis of airflow structure allows for better understanding of the aerodynamic phenomena that is the origin of noise source and provides design information to improve and optimize the side mirrors. In this paper, the focus lies on the aerodynamic noise simulation by analyzing the turbulent flow structure and predict the external acoustic field using $k - \epsilon$ and LES turbulent modeling approaches. The numerical results are compared to the experimental results with only 6.7% error in static pressure on the mirror surfaces. The simulation results showed that the spectra of sound pressure level with LES model is close to experimental data than that with $k - \epsilon$ model.

Keywords: Car side mirror, RANS, LES, static pressure, sound pressure level.

1. Introduction

In recent decades, with the rapid development of computation power and modeling methods for turbulent flow simulation problems, the field of Computational Aero Acoustic (CAA) became more and more relevant for the industrial applications, such as, aerospace engineering or civil engineering. The initial studies focused only on the aerospace field, but more and more researches focus in the industry sector automobile technology.

The aerodynamic noise generation [1-8] caused by the turbulent flow around the car was simulated. The zone of generic side mirror [4-5, 9-11] is one of the sensitivity zones in which the flow is separated and detached from the flat side of the mirror. Evaluation of experimental results presented by Barnard [12], from a performance point of view, the contribution of a generic side mirror to total drag of a car was between 3% and 6% (this is a considerable percentage if comparing the volume of side mirror with total vehicle). The turbulence created by this flow is the noise sources. In the car types, the driver's position was fixed and not perpendicular to the mirror which should be placed so that drivers can be having the biggest angle cover behind direction. In fact, the angle of mirror with the perpendicular of car door is around 15° - 30° depending on the vehicle types (sport or passenger). The numerical results in [7-10] were studied with the mirror angle of 0° (the mirror is perpendicular of car door). In this work, the simple design base on the real case that this angle is of 22.5° .

The transient airflow was numerically simulated with LES (Large Eddy Simulation) turbulent model [6-10] in a commercial computational fluid dynamics program, ANSYS-Fluent. However, the calculation time is too long, and the computational cost is increased.

In the present work, the CAA process was implemented coupling between the $k - \epsilon$ and LES turbulent models to understand the nature of an aero acoustic phenomenon of airflow around the car side mirrors with a low cost of calculation in time and computer performance, the numerical results of side mirror are also presented in comparison with the experiment data.

2. Numerical Analysis

2.1. Description of Geometry

The goal of this part is to understand the nature of the aero acoustic phenomena (noise source from turbulent airflow) of airflow around the car side mirrors. The CAA process starts with the simple geometry, in order to reduce the complexity of the system, the simple geometry of side mirror is based on the quarter of the sphere mounted on a half-elliptical cylinder as shown in Fig. 1.

Based on the real size of a car side mirror, the geometry of a simple side mirror used in this study consisted of quarter-elliptical sphere with the radius $R_a = 0.1\text{ m}$ and $R_b = 0.07\text{ m}$ on a half-elliptical cylinder with the radius $R_a = 0.1\text{ m}$ and $R_b = 0.07\text{ m}$,

and height $h = 0.2 \text{ m}$. Ignoring the effects of the car body on the airflow and aero acoustic field around the side mirror zone, the side mirror was mounted on a vertical wall as car window. The uniform velocity in inlet section of 38.9 m/s is used for this study

equivalent to a car speed of nearly 140 km/h , which correspond approximately to Reynolds number of $6,325,420$ for this test case.

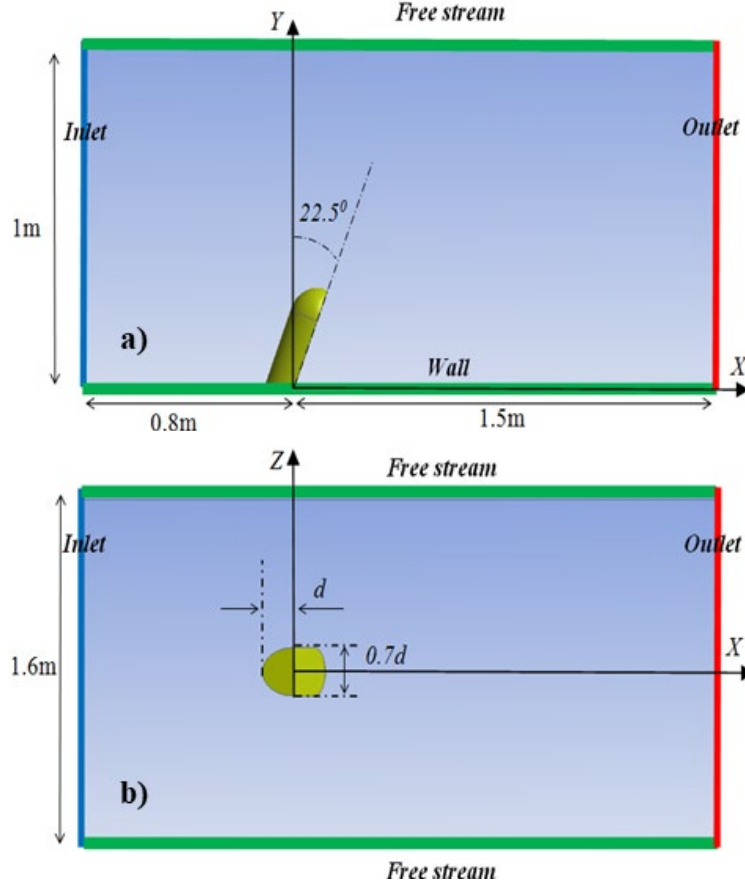


Fig. 1. Problem domain and boundary condition: a) Side view and b) Plan view

2.2. Turbulent and Acoustic Models

The flow structure in the wake of the side mirror is highly transient and will generate strong pressure fluctuation on the door panels and the window. This unsteady pressure fluctuation is the source exterior noise. Some turbulence models are used in [3-6, 13-14] for analyzing the unsteady flow around the side mirror. On the other hand, working experience as well as literature studies show that a simple turbulent model using the Navier-Stokes equations, like $k - \epsilon$, $k - \omega$ and SST models, does not resolve the time dependent nature of the flow properly for all relevant scales, and is not really suitable for aero acoustic computation. The results in [6, 15-16] show that the LES (Large Eddy Simulation) is the better for resolving separated and detached airflow around the side mirror, that is also the choice of this research.

The basic equations used in this simulation are as following.

Continuity equation:

$$\frac{\partial \rho}{\partial t} + \frac{\partial(\rho u_i)}{\partial x_i} = 0 \quad \frac{\partial \rho}{\partial t} + \frac{\partial(\rho u_i)}{\partial x_i} = 0 \quad (1)$$

Momentum equation:

$$\frac{\partial(\rho u_i)}{\partial t} + \frac{\partial(\rho u_i u_j)}{\partial x_j} = -\frac{\partial \rho}{\partial x_i} + \frac{\partial}{\partial x_i} \tau_{ij} + \rho g \quad (2)$$

where:

$$\tau_{ij} = \mu \left(\frac{\partial u_i}{\partial x_j} + \frac{\partial u_j}{\partial x_i} \right) - \frac{2}{3} \frac{\partial u_k}{\partial x_k} \delta_{ij}$$

is the viscous stress tensor for a Newtonian fluid. ρ , μ , and u are the density, dynamic viscosity coefficient and velocity of airflow.

Depending on the state of airflow, the viscous stress tensor is closed differently, the viscous stress tensor is decomposed in two terms: one is viscous tensor and other is Reynolds's tensor.

If the airflow is incompressible, we have following tensors.

Viscous tensor:

$$\overline{\tau_{il}} = \mu \left(\frac{\partial \overline{u_i}}{\partial x_l} + \frac{\partial \overline{u_l}}{\partial x_i} \right) \quad (3)$$

Reynolds's tensor:

$$-\overline{\rho u_i u_l} = \mu_T \left(\frac{\partial \overline{u_i}}{\partial x_l} + \frac{\partial \overline{u_l}}{\partial x_i} \right) - \frac{2}{3} \rho k \delta_{il} \quad (4)$$

where μ_T is the eddy viscosity and $-\frac{2}{3} \rho k \delta_{il}$ is additional term required for consistency with the definition of k (turbulent kinetic energy).

If the airflow is compressible, using the Stokes' hypothesis, the viscous tensor is written as

$$\overline{\tau_{il}} = \tilde{\mu}(\tilde{T}) \left[\frac{\partial \tilde{u}_i}{\partial x_l} + \frac{\partial \tilde{u}_l}{\partial x_i} \right] - \frac{2}{3} \tilde{\mu}(\tilde{T}) \frac{\partial \tilde{u}_k}{\partial x_k} \delta_{il} \quad (5)$$

with

$$\tilde{\mu}(\tilde{T}) = \mu_{273} \left(\frac{\tilde{T}}{273.15} \right)^{3/2} \frac{110.4 + 273.15}{110.4 + \tilde{T}}$$

Using the Boussinesq's hypothesis in compressible with the dissipation rate of turbulence (ε), the Reynold's tensor is written as:

$$\overline{\rho u_i u_l} = \mu_T \left(\frac{\partial \tilde{u}_i}{\partial x_l} + \frac{\partial \tilde{u}_l}{\partial x_i} \right) - \frac{2}{3} \mu_T \frac{\partial \tilde{u}_k}{\partial x_k} \delta_{il} - \frac{2}{3} k \delta_{il} \quad (6)$$

with $\mu_T = C_\mu \tilde{\mu} R_{eT} \mu_T = C_\mu \tilde{\mu} R_{eT}$; $C_\mu = 0.09$ and $R_{eT} = \frac{k^2}{\tilde{\nu} \varepsilon}$

The $k - \varepsilon$ and LES turbulent models were introduced in the most of works [4-8, 15, 17-18] that author used in this article.

The aero acoustic modeling and simulation are used the Ffowcs-Williams-Hawkins acoustic analogy by using the Lighthill's equation that is presented in [1, 2, 7, 8, 18].

The process of airflow simulation is done first using $k - \varepsilon$ model for steady state, that assuming the flow is incompressible. This steady state solution is taken premise for transient LES where the airflow is compressible.

2.3. Numerical Method

To reduce the cost software and simplicity in their uses, we use the module Design Modeler available in ANSYS Workbench 19.1 [19] to build the simulation models. The use of modules available in ANSYS helps more smoothly research, especially when we use the module Design Exploration to study the effects of design changes on the airflow and acoustics field. Several test geometries and varying angles of attack were studied pending the simulation study, but the current setup for experiment was the one

chosen as the most representative of this class of flows and correspond with the real case test.

The mesh was created in the module available commercial software ANSYS 19.1, ICEM. A hexahedral mesh was constructed in the entire domain with coarse mesh in the far zone and mesh cluster in the near zone of side mirror as in Fig. 2 where the pure hexahedral mesh is represented. In this paper, the main research interest is only around the side mirror, so that the mesh will be generated to reduce the computation and convergence times, and to evaluate the aerodynamic and aeroacoustic phenomenon of flow. So here, we also provide a grid independency test in this research for studying the effect of mesh on the convergence of the results. The total of 2 million elements is limit of the calculation that depends on calculation time, this limit is corresponds with cubic cells 1 mm adjacent to the solid wall. With the bias technique mesh, the cubic cells are smaller than 1 mm to a side with the same elements of cubic. However, the use of this technology makes computing time increase because the airflow element in the calculation is not entirely the same.

In the simulation model, the mirror is placed 80 cm from the inlet section, this allows us to specify the inlet properties unambiguously. The lateral and top boundaries are implemented as symmetry planes. The location of the symmetry planes is chosen far enough from the mirror body so that the effects of blockage will be minimal (less than 4%). The outlet is a standard convective boundary located at a position downstream where no reverse flow or zero-gradient assumptions will affect statistics in the measured region (atmospheric condition). The base plate and mirror surface are no-slip impermeable walls with instantaneous wall functions used to provide the tangential shear stress at the surface.

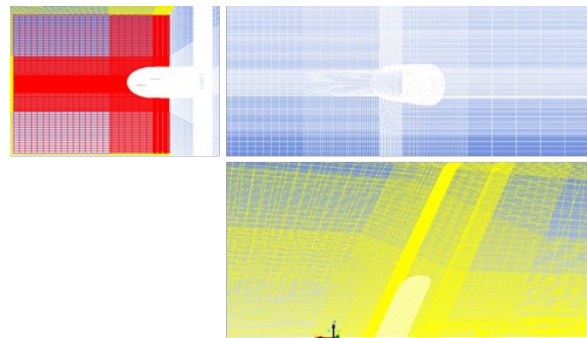


Fig. 2. Computational flow mesh

The boundary conditions for the different surfaces bounding are listed as in the Table 1. The peak and near-stall conditions were defined as the points where the maximum adiabatic efficiency and maximum total pressure ratio are achieved, respectively. The stall margin is a measure of how far the peak point is to near-stall point. The stable range extension is the increase in the stable operating range

(between choke and near-stall) of the case with recirculation channel as compared to the smooth case.

Table 1. Boundary Conditions

Boundary Name	Boundary Condition	Value
Inlet	Constant velocity	38.9 (m/s)
Outlet	Constant Pressure	0 (Pa)
Free stream	Far field	-
Wall	Wall (No Slip)	
Mirror	Wall (No Slip)	

3. Result and Discussion

The simulation was used with the ANSYS FLUENT 19.1 by using an eight-core 3 GHz workstation with 16 Gb RAM. Approximately 20 days were needed to finish the simulation. The static pressure was monitored at the point of 20 mm perpendicular of rear surface in the wake of the mirror, this point is totally in the turbulent zone. It is a transition step to aero acoustic simulation because for aero acoustic simulation, it is obligatory that the pressure is completely converged at the receiver position.

Before going into analyze and evaluation of turbulent airflow structures as well as the aeroacoustic phenomenon, we give some comments on the influence of the mesh on the convergence results of the static pressure of some characteristic points in the airflow.

Fig. 3 shows that the difference between CFD solution of maximal static pressure on Mirror was negligible after 1,400,000 nodes. However, this value decreased slightly when it is asymptotically to the optimal value of 1,160 Pa with approximately 2 million elements. Hence, no further meshing refinement was needed. Finally, the mesh with 1,400,000 nodes was used for all cases.

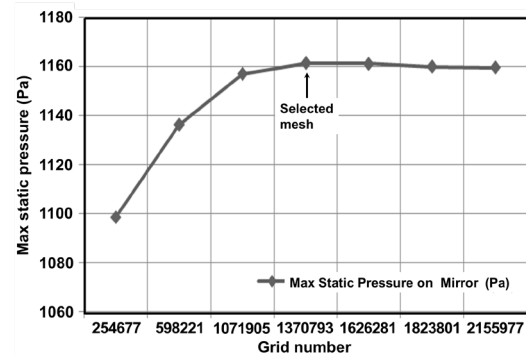


Fig. 3. Grid independence test

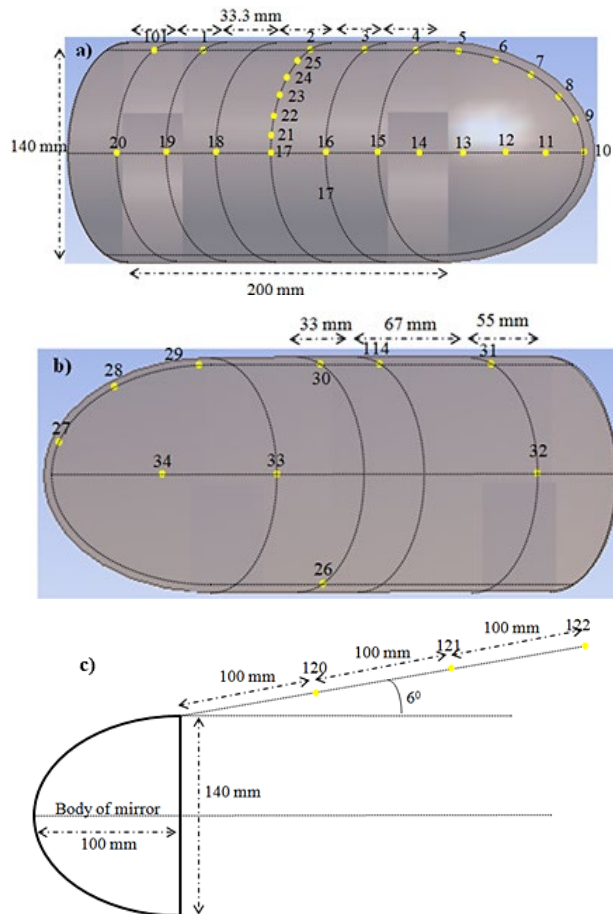


Fig. 4. Probe locations: a) Front mirror surface, b) Rear mirror surface, c) In the mirror wake on the plane at $z = 150$ mm

Three probe points were located and illustrated in Fig. 4, where three points were used one on front of mirror; one on top of mirror and one in the wake zone on behind the mirror: 101, 114 và 122. The simulation procedure was as follows: a converged *RANS* solution based on the $k - \epsilon$ model served as an initial condition. After this initialization, a coarse time step was first chosen to convert free stream disturbances downstream. The time step at this stage was 0.001s, and the simulation was run until the drag coefficient of the mirror and static pressure of receivers were stable and their fluctuations were around their average values, equivalent to about 100-time steps (0.1s) as in the Fig. 5 below for the fine mesh (2 million nodes).

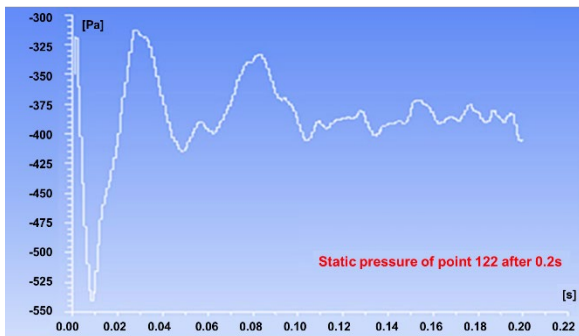


Fig. 5. Convergence history of static pressure on point 122 (in the wake zone)

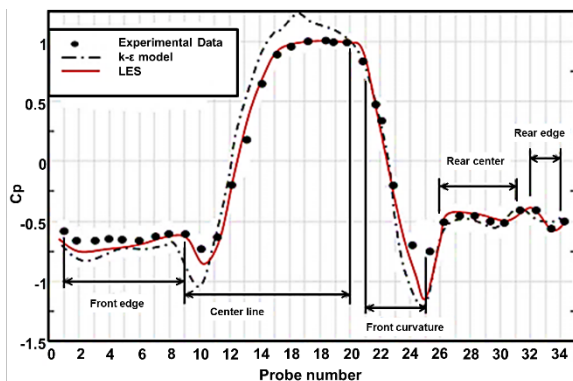


Fig. 6. Comparison of static pressure at selected probe locations on the mirror surface

After identifying the salient features and dynamics of flow around the mirror, we can now provide a quantitative comparison of LES model selected properties with the experimental data. Fig. 6 shows that the static pressure of probe points is similar with experiments. However, in the $k - \epsilon$ model, the redistribution term is negligible ($\phi_{ii} = 0$), so it cannot predict important recirculation zone. The choice of LES model allows to capture the dynamics of the free shear layer encapsulating the recirculation zone behind the mirror. The experimental results of static pressure were reported by Hoeld *et al.* [4] and Siegert *et al.* [5]. As shown in Fig. 6, the different value of static pressure with LES and experimental results was highest near the front curvature and rear center. The

maximal different value of static pressure with LES and experimental results reaches 6.7% on the front edge of the mirror.

3.1. Flow Features and Dynamics

The results are further divided into mean and instantaneous results, followed by the time-dependent results. The flow is dominated by a large recirculation zone behind the mirror. Other features of note include a horse-shoe shaped vortex that wraps around the front of the mirror and an extensive V-shaped wake region downstream of the recirculation zone. The flow is dominated by a large recirculation zone behind the mirror. Other features of note include a horse-shoe shaped vortex that wraps around the front of the mirror and an extensive V-shaped wake region downstream of the recirculation zone.

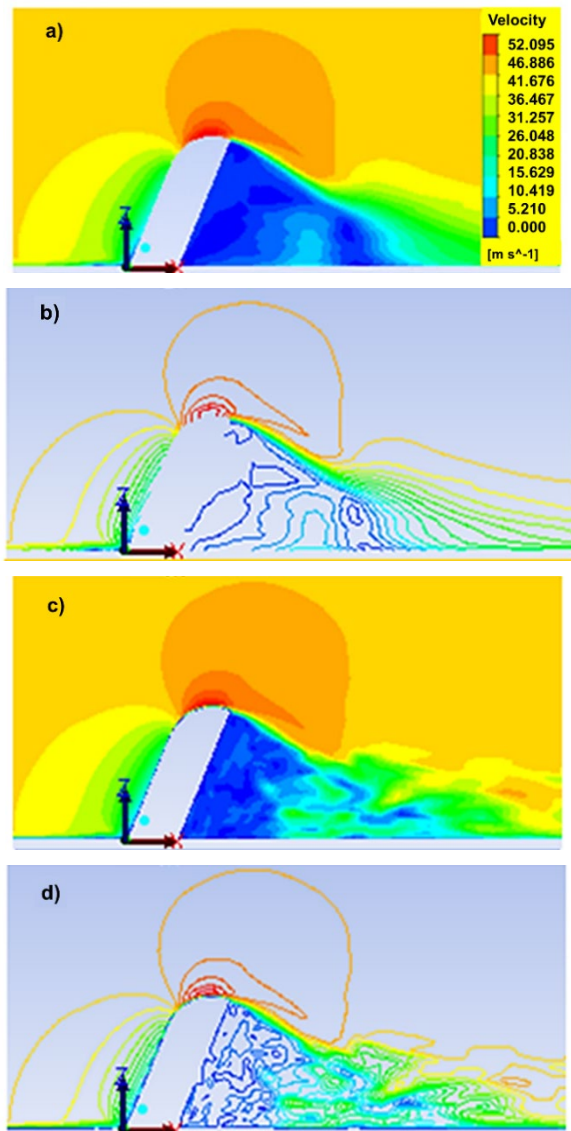


Fig. 7. Centre-line velocity and contour:
 a) Mean velocity magnitude, b) Mean contour,
 c) Instantaneous velocity magnitude, and
 d) Instantaneous contour

Fig. 7 shows the distributions in the symmetry plane passing through the mirror, from which the extent and properties of the recirculation and turbulent zone are readily apparent.

3.2. Pressure Spectra - Aeroacoustic

The main proposes of this investigation is to evaluate the capabilities of LES model as an aeroacoustic noise source predictor. The basic for the simulation of the origin and propagation of sound is using the Ffowcs-Wiliams-Hawkins acoustic analogy that is derived from the basic Navier-Stokes equations. The sound pressure level (SPL) is calculated by:

$$SPL = 10 \times \log\left(\frac{p'^2}{p_0^2}\right)$$

where p_0 is the reference pressure and it is equal to $2 \times 10^{-5} Pa$, p' is the sound pressure (fluctuating pressure) and the sound pressure level has units of decibel [dB], which is commonly used to specify the sound level. Fig. 8 shows the maximum of power noise source is on the front face of mirror where the flow stagnation occurs. The power noise generating energy is high on the rear face of mirror, this phenomenon is

explained by the collision of airflow in the behind on the rear surface of mirror.

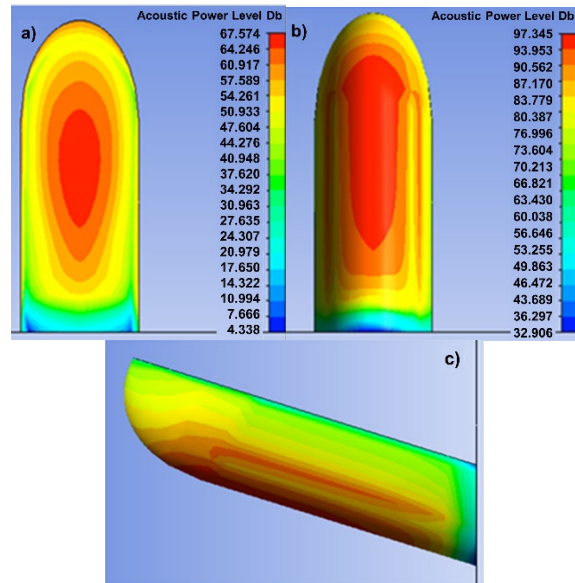


Fig. 8. Noise source on side mirror: a) rear surface, b) front surface, c) side surface

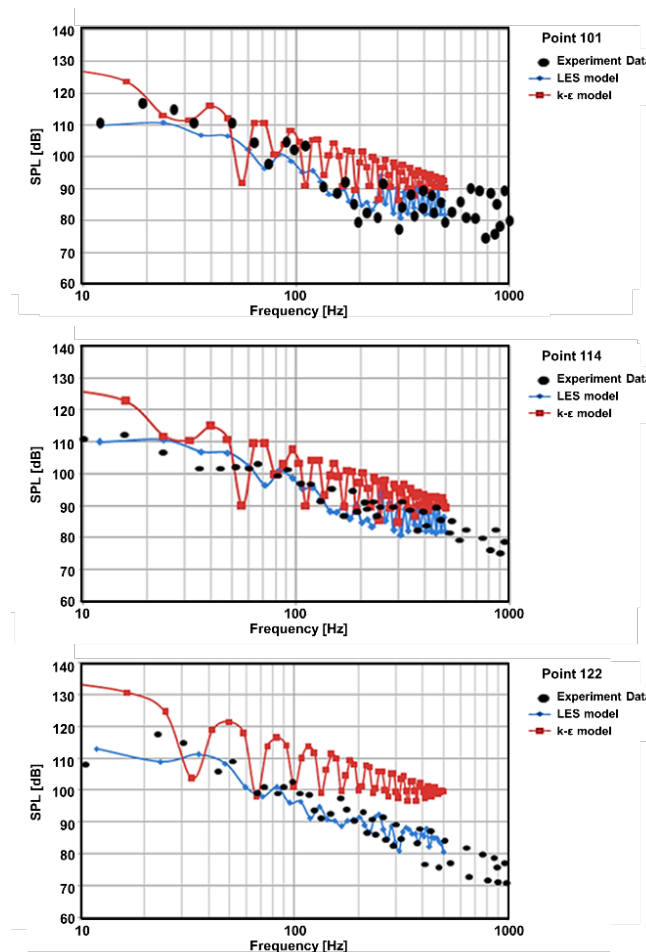


Fig. 9. Spectra of SPL: a) Point 101, b) Point 114, and c) Point 122

The experimental results of SPL were reported by Hoeld *et al.* [4] and Siegert *et al.* [5]. Fig. 9 shows the noise at different points (Fig. 4) on front (point 101), on rear (point 114), and in the wake zone of mirror (point 122). These figures show that the LES model allows well predict the aeroacoustic flow that the SPL close to the parallel experiments. The numerical variable regions of SPL are within the experimental results. Whereas, the $k - \varepsilon$ model's results are not closed to the experimental values.

4. Conclusion

The main goal of this paper was to determine the applicability and practicality the LES methodology for the prediction of aerodynamic properties and SPL production in an automotive environment. The $k - \varepsilon$ model is also used in this paper to compare and evaluate its advantages and disadvantages with the LES model. The results have demonstrated that the LES model is appropriate for predicting the static pressure on the car side mirror surface and the SPL of the car side mirror. The numerical results with LES model are compared to the experimental results with only 6.7% error in static pressure on the mirror surfaces. The SPL of three points (Point 101, Point 114 and Point 122) with LES model are closed to the parallel experiments. The next work of this paper is to use LES model for design optimization of the mirror to minimize noise and improve the aerodynamic characteristics of the mirror in the different speed.

Acknowledgment

This study is funded by the by Hanoi University of Science and Technology (HUST) under grant number T2021-PC-039.

Reference

- [1] M. J. Lightthill, On sound generated aerodynamically, I. General theory, Proc. Roy. Soc., Vol. 211, No. 1107, pp. 564-587. 1952, <https://doi.org/10.1098/rspa.1952.0060>
- [2] J. E. Ffowcs Williams and D. L. Hawkins, Sound generation by turbulence and surfaces in arbitrary motion sound, Philos. Trans. Roy. Soc., Vol. 264, No. 1151, pp. 321-342. 1969, <https://doi.org/10.1098/rsta.1969.0031>
- [3] H. Fujita, W. Sha, H. Furutani, H. Suzuki, Experimental investigations and prediction of aerodynamic sound generated from square cylinders, 4th AIAA/CEAS Aeroacoustics Conference, Toulouse, France, pp. 942-947. 1998, <https://doi.org/10.2514/6.1998-2369>
- [4] R. Hoeld, A. Brenneis, A. Eberle, V. Schwarz, R. Siegert, Numerical simulation of aeroacoustic sound generated by generic bodies placed on a plater: Part I - prediction of aeroacoustic sources, In 5th AIAA/CEAS Aeroacoustic Conference. Bellevue, Washington, USA. 1999, <https://doi.org/10.2514/6.1999-1896>
- [5] R. Siegert, V. Schwarz, J. Reichenberger, Numerical simulation of aeroacoustic sound generated by generic bodies placed on a plater: Part II - prediction of radiated sound, In 5th AIAA/CEAS Aeroacoustic Conference. Bellevue, Washington, USA. 1999, <https://doi.org/10.2514/6.1999-1895>
- [6] J. Ask, L. Davidson, The Sub-critical flow past a generic side mirror and its impact on sound generation and propagation, collection of technical papers - 12th AIAA/CEAS Aeroacoustics Conference, Cambridge, Massachusetts, USA. 2006, <https://doi.org/10.2514/6.2006-2558>
- [7] T. Grahs, C. Othmer, Evaluation of aerodynamic noise generation: parameter study of a generic side mirror evaluating the aeroacoustic source strength, Proceedings of the European Conference on Computational Fluid Dynamics (ECCOMAS CFD 2006), Delft University of Technology, Delft, Netherlands. 2006,
- [8] Y. Wang, Z. Gu, W. Li, X. Lin, Evaluation of aerodynamic noise generation by a generic side mirror, world academy of science, engineering and technology, International Journal of Aerospace and Mechanical Engineering, Vol. 4, No. 1, pp. 120-127. 2010,
- [9] B. Lokhande, S. Sovani and J. Xu, Computational Aeroacoustic Analysis of a Generic Side View Mirror, SAE Technical Papers. Paper No. 2003-01-1698. 2003, <https://doi.org/10.4271/2003-01-1698>
- [10] I. Afgan, C. Moulinec and D. Laurence, Numerical simulation of generic side mirror of a car using large eddy simulation with polyhedral meshes, International Journal for Numerical Methods in Fluids, Vol. 56(8), pp. 1107-1113. 2008, <https://doi.org/10.1002/flid.1719>
- [11] J. H. Kim, Y. O. Han and B. D. Lim, 2009 Experimental study of statistical and spectral characteristics of wake flow around the rear-view side mirror of a passenger car, Proceedings of 5th European and African Conference on Wind Engineering, EACWE 5, Florence, Italy.
- [12] R. H. Barnard, 1988, Road Vehicle Aerodynamic Design: An Introduction, Longman: New York, USA.
- [13] T. Rung, D. Eshricht, J. Yan and F. Thiele, 2002, Sound Radiation of the Vortex Flow Past a Generic Side Mirror, 8th AIAA/CEAS Aeroacoustics Conference & Exhibit, Breckenridge, Colorado, USA. <https://doi.org/10.2514/6.2002-2549>
- [14] T. Uffinger, S. Becker, D. Antonio, Investigations of the flow field around different wall-mounted square cylinder stump geometries, 14th International Symposium on Applications of Laser Techniques to Fluid Mechanics, Lisbon, Portugal. 2008,
- [15] P. Spalart, W. H. Jou, M. Strelets, S. Allmaras, 1997, Comment on the feasibility of LES for wing, and on a hybrid RANS/LES approach, In Advances in DNS/LES First AFOSR International Conference on DNS/LES, Greyden Press.

- [16] F. Menter, M. Kuntz and R. Bender, A scale-adaptive simulation model for turbulent flow prediction, 41st Aerospace Sciences Meeting and Exhibit, Reno, Nevada, USA. 2003, <https://doi.org/10.2514/6.2003-767>
- [17] M. Escobar, I. Ali, C. Hahn, M. Kaltenbacher, S. Becker, Numerical and experimental investigation on flow induced noise from a square cylinder, Collection of Technical Papers - 10th AIAA/CEAS Aeroacoustics Conference. 2004, <https://doi.org/10.2514/6.2004-3004>
- [18] X. Chen, S. Wang, Y. Wu, Y. Li, Wang, H. Wang, Experimental and numerical investigations of the aerodynamic noise reduction of automotive side view mirrors, Journal of Hydrodynamics, Vol. 30(4), pp. 642-650. 2018, <https://doi.org/10.1007/s42241-018-0070-1>
- [19] ANSYS CFX-19.1, 2018, ANSYS Inc.